Soft Matter

Accepted Manuscript

ROYAL SOCIETY OF CHEMISTRY

www.rsc.org/softmatter

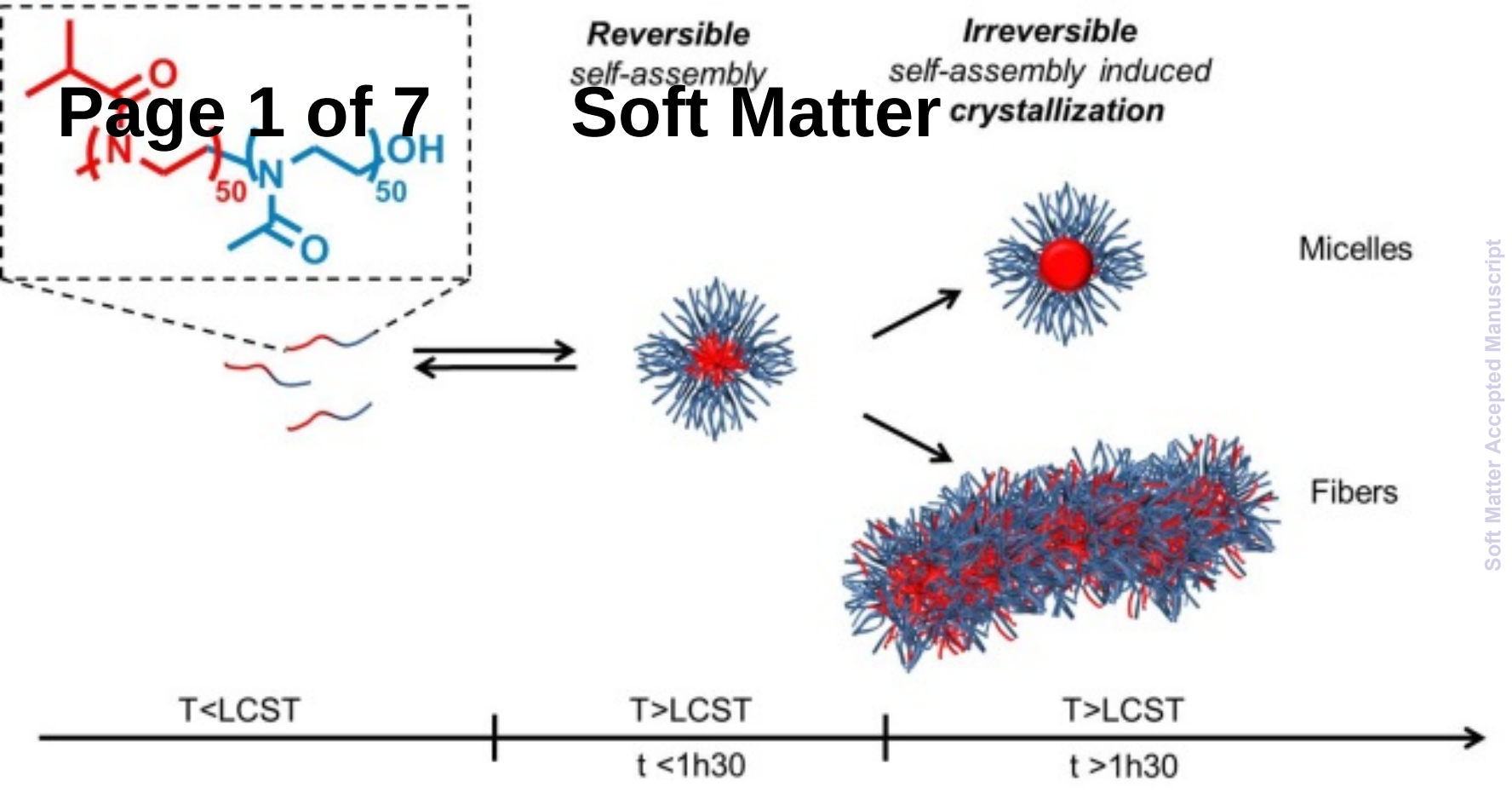

Journal Name

RSCPublishing

ARTICLE

Crystallisation-driven self-assembly of poly(2-isopropyl-2-oxazoline)-block-poly(2-methyl-2-oxazoline) above the LCST

Cite this: DOI: 10.1039/x0xx00000x

Received 00th January 2012,
Accepted 00th January 2012

DOI: 10.1039/x0xx00000x

www.rsc.org/

Camille Legros,[abcd] Marie-Claire De Pauw-Gillet,[d] Kam Chiu Tam,[c] Daniel Taton*[ab] and Sébastien Lecommandoux*[ab]

The solution behaviour in water of a polyoxazoline-type block copolymer, namely poly(2-isopropyl-2-oxazoline)-*block*-poly(2-methyl-2-oxazoline), denoted as P(iPrOx-*b*-MeOx), above the lower critical solution temperature (LCST) of the PiPrOx block was exploited to induce a temporary or permanent self-assembly. Spherical micelles were first obtained and could be disassembled in a reversible manner when kept for a short period of time (*i.e.* t < 90 min) above the LCST, and cooled down to room temperature. In contrast, annealing the copolymer solution for more than 90 min at 65 °C induced the crystallisation of the PiPrOx block, as evidenced by wide angle X-ray scattering (WAXS) experiments. This crystallisation-driven self-assembly phenomenon resulted in different morphologies, including spherical and distorted crystallised micelles and micron-size fibers, their relative proportion varying with annealing time. Formation of micron-size range fiber-like structures might be explained by a re-organization of parent crystallised micelles. The crystal structure, as determined by WAXS, appeared to be identical to that of the PiPrOx homopolymer.

Introduction

As a result of the different solubility between at least two polymer chains, block copolymers (BCP) can self-assemble in solution into well-defined micellar nanostructures of different shapes.[1,2] In many cases, self-assembly is driven by hydrophobic interactions. Some examples can also be found where self-assembly is driven by electrostatic interactions between a pair of oppositely charged BCP, or BCP with complementary chirality. However, when multiple forces are involved, more complex nanostructures can be achieved.[2] Starting about a decade ago, the self-assembly of semi-crystalline BCP containing at least one crystallisable block has been studied in depth.[3,4] From this crystallisation driven self-assembly (CDSA) of BCP containing crystalline blocks, such as polyolefins,[5–9] polyferrocenylsilane,[10–15] poly(ethylene oxide),[16–19] or poly (*L*-lactide),[20–23] a library of hierarchical crystalline structures have been achieved, including elliptical, spherical, cylindrical, worm-like, disk-like micelles, and polymeric crystalline vesicles as well. Morphologies obtained could be tuned depending on the polymer composition (di- or tri-block, block length/ratio) and on experimental conditions such as the temperature or the solvent used. The "living" character of the CDSA process was also highlighted for some systems where the epitaxial growth of BCP onto a preformed crystalline micellar nano-structure was possible.[7,24] Various micellar morphologies have also been observed from CDSA of a peculiar crystalline-crystalline BCP, namely, poly(ethylene oxide)-*block*-poly(caprolactone).[24–27]

In the present work, the CDSA has been investigated for the first time with a particular polyoxazoline (POx)-based BCP. Formation of physically cross-linked, or frozen structures at the nano- and the micron-size range have thus been observed. The versatility of POx, associated with their interesting biological properties (structural similarities with polypeptides,[28] biocompatible character and stealth behaviour of some POx[29–31]) has led to their recent revival. The cationic ring-opening polymerization (CROP) of 2-alkyl-2-oxazolines has been adapted for the synthesis of well-defined (co)polymers the physico-chemical properties of which could be finely tuned.[32–34]

Among 2-alkyl-2-oxazoline monomers, 2-isopropyl-2-oxazoline (iPrOx) is of particular interest. The resulting polymer, PiPrOx, is indeed a structural isomer of poly(N-isopropylacrylamide) (PNIPAAm). Like PNIPAAm, PiPrOx exhibits a lower critical solution temperature (LCST) in water around 36 °C,[35] which makes it a good candidate for the design of thermo-responsive polyoxazoline-based compounds. In addition, and in contrast to PNIPAAm, PiPrOx is capable of crystallising above its LCST.[36] The advantage of such a behaviour has been reported by Schlaad *et al.* who have observed hierarchical structures, such as micron-size assemblies of fibrils from PiPrOx homopolymer.[37,38] The

morphology eventually proved to evolve with time, from network-like structures into micron-size assemblies.[39] A statistical copolymer made of iPrOx and 2-(3-butenyl)-2-oxazoline units has been also found to self-assemble and crystallise above its LCST into spherical micron-size structures.[40] Self-assembly and crystallisation of a PiPrOx-*graft*-pullulan copolymer has been also reported.[41] PiPrOx is not the only POx that can undergo crystallisation. Chiral POx,[42] PEtOx[43] and some homopolymers with side chains of different linear alkyl length[44] can also crystallise upon annealing. In addition, poly(2-isobutyl-2-oxazoline) and poly(2-nonyl-2-oxazoline) were also found to crystallize after room temperature annealing below the upper critical solution temperature in ethanol-water solvent mixtures.[45]

In this work, PiPrOx was organised for the first time into a block copolymer architecture associated with a poly(2-methyl-2-oxazoline) (PMeOx) block. The specific properties of each block (crystallisation and LCST for PiPrOx on one hand, and water-solubility for PMeOx on the other hand) were thus combined, with the aim of investigating the crystallisation-driven self-assembly of the P(iPrOx$_{50}$-*b*-MeOx$_{50}$) BCP, above the LCST of PiPrOx, and the possible stabilizing effect of PMeOx.

Experimental section

Materials

2-Methyl-2-oxazoline (99%) (EtOx), methyl trifluoromethanesulfonate (96%) (MeOTf), and acetonitrile (99%) were purchased from Sigma-Aldrich, stored over calcium hydride and purified by vacuum distillation prior to use. Methanol purchased from Aldrich was refluxed with sodium and distilled prior to use. Diethyl ether, potassium hydroxide (KOH), isobutyronitrile (99.6%) and cadmium acetate dehydrate (98%) were purchased from Sigma-Aldrich and used as received. 2-Amino-ethanol was purchased from Fisher Scientific.

Analytical instrumentation and characterization techniques

NMR spectroscopy. ^{1}H NMR measurements were carried out at 298K on a Bruker Avance I spectrometer operating at 400 MHz. $CDCl_3$ or D_2O were used as an internal reference (δ = 7.26 and 4.79 ppm respectively), and the relaxation time was fixed to 5 sec for all measurements.

Size-exclusion chromatography. Size-exclusion chromatography (SEC), using dimethylformamide (DMF) with LiBr (1 g/L) as the eluent, was performed at 80 °C, at a flow rate of 0.8 mL/min. The column set consisted of two 7.5 mm × 300 mm PLgel, 5 µm Mixed-D columns (Polymer laboratories) coupled to a 7.5 mm × 50 mm, PLgel, 5 µm guard column (Polymer laboratories). A 20 µL injection loop was used and calibration was performed with polystyrene standard. Differential refractive index (RI) and UV detectors were used.

Dynamic light scattering. Dynamic light scattering (DLS) measurements were run in triplicate on a Malvern Zetasizer apparatus (Nano-ZS90 model), at a back scattering angle of 90°.

Transmission electron microscopy. Transmission Electron Microscopy (TEM) images were recorded at Bordeaux Imaging center (BIC) on a Hitachi H7650 microscope working at 80 kV. Samples were prepared by drop depositing 0.7 µL of a 0.05 wt% of the desired copolymer solution onto a copper grid (200 mesh coated with carbon) and removing the excess after 5 minutes. In order to image the reversible micelles observed only above the LCST of the copolymer, the grid was left to dry at 65 °C (*i.e.* above the LCST). Statistical size analyses of particles observed by TEM were carried out using Image J.

Wide angle X-ray scattering. Wide angle X-ray scattering experiments (WAXS) were carried out at the Centre de Recherche Paul Pascal (CRPP, Pessac, France). Measurements were carried out on a Rigaku Nanoviewer (XRF microsource generator, MicroMax 007HF) with a rotating copper anode coupled to a confocal Osmic Max-Flux mirror (Applied Rigaku Technologies, Austin, USA), producing a beam with a wavelength of 1.5418 Å with an energy of 8 keV. Data were collected with a Mar345 detector (Marresearch, Norderstedt, Germany). Polymer solutions were freeze-dried and put into a 1.5 mm diameter glass capillary, placed at a distance of 150 mm away from the detector (diameter of 345 mm), providing access to 2θ angles in the range of 0.9° to 49°.

Experimental procedures

Synthesis of 2-isopropyl-2-oxazoline (iPrOx). 2-Isopropyl-2-oxazoline (iPrOx) was synthesized as described elsewhere:[46]
51g of 2-amino-ethanol (0.83 mol) was added drop-by-drop to a suspension of 54.5 g of isobutyronitrile (0.79 mol) and 10.65 g of cadmium acetate dihydrate (0.04 mol) at 130 °C. The solution was stirred for 24 h at 130 °C and then fractionated by vacuum distillation. Yield: 64 g (0.57 mol, 72%). ^{1}H NMR (400 MHz, D_2O, δ): 1.1 (d, 6H, CCH(C*H*$_3$)$_2$), 2.35 (m, 1H, CC*H*(CH$_3$)$_2$), 3.7 (t, 2H, OCH$_2$C*H*$_2$N), 3.96 (t, 2H, OC*H*$_2$CH$_2$N).

Synthesis of poly[(2-isopropyl-2-oxazoline)$_{50}$-*block*-(2-methyl-2-oxazoline)$_{50}$] (P(iPrOx$_{50}$-*b*-MeOx$_{50}$)). A typical procedure is as follows: in a flame dried Schlenk flask, 6.6 mL of acetonitrile was introduced under vacuum. 28.3 µL (0.25 mmol) of MeOTf was added. The flask was then placed in an ice bath at 0 °C and 1.48 mL (12.5 mmol) of 2-isopropyl-2-oxazoline was added. The flask was then maintained at 85 °C for 3 days, until complete consumption of the monomer (monitored by ^{1}H NMR spectroscopy). 1mL of 2-methyl-2-oxazoline (11.7 mmol) was added and the reaction was quenched by adding 2.7 equivalents of a 0.3N KOH solution in methanol at 95% conversion (determined by ^{1}H NMR spectroscopy). The solution was left to stir at room temperature overnight and the polymer was precipitated twice into diethyl ether and dried under vacuum. Yield = 2.08 g (89 %). ^{1}H NMR (400 MHz, D2O, δ): 3.7-3.3 (s, NCH$_2$CH$_2$), 3.1 (s, CH$_3$-NCH$_2$CH$_2$), 3.0-2.55 (d, COCH(CH$_3$)$_2$), 2.2-2.0 (m, NCOCH$_3$), 1.15-1 (s, NCOCH(CH$_3$)$_2$). *Đ* = 1.19.

~~**Synthesis of poly[(2-methyl-2-oxazoline)$_{50}$-*block*-(2-sopropyl-2-oxazoline)$_{50}$] (P(MeOx$_{50}$-*b*-IPrOx$_{50}$)).** The same procedure, as described above for P(iPrOx$_{50}$-*b*-MeOx$_{50}$) was also used to synthesize P(MeOx$_{50}$-*b*-IPrOx$_{50}$), except that monomers were added in the reverse order. Yield = 1.15 g (47 %). ^{1}H NMR (400 MHz, D_2O, δ): 3.7-3.3 (s, NC*H*$_2$C*H*$_2$), 3.1 (s, C*H*$_3$-NCH$_2$CH$_2$), 3.0-2.55 (d, COC*H*(CH$_3$)$_2$), 2.2-2.0 (m, NCOC*H*$_3$), 1.15-1 (s, NCOCH(C*H*$_3$)$_2$). *Đ* = 1.33. DP(MeOx) = 52, DP(iPrOx) = 50.~~

Results and discussion

Synthesis of P(iPrOx$_{50}$-*b*-MeOx$_{50}$) copolymers by cationic ring opening polymerization

The P(iPrOx$_{50}$-*b*-MeOx$_{50}$) BCP was obtained by sequential CROP of corresponding 2-oxazoline monomers, using methyl trifluoromethanesulfonate (MeOTf) as the initiator, after 3 days

at 85 °C in acetonitrile (ACN; Scheme 1). The compound was characterized by a dispersity of 1.19 and a degree of polymerization of 50 for each block.[47]

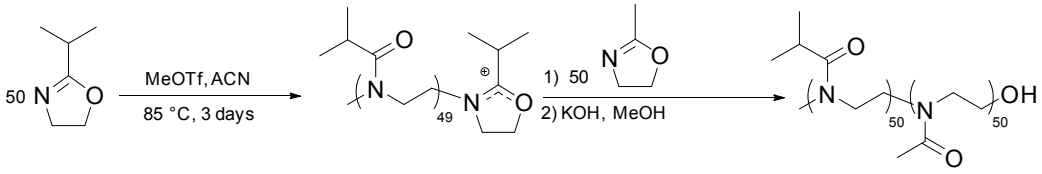

Scheme 1 Synthesis of P(iPrOx$_{50}$-*b*-MeOx$_{50}$) by sequential cationic ring-opening polymerization

Reversible self-assembly of P(iPrOx$_{50}$-*b*-MeOx$_{50}$) above the LCST

The cloud point of a 10 mg/mL solution of P(iPrOx$_{50}$-*b*-MeOx$_{50}$) was found to be around 57 °C, as determined by dynamic light scattering measurements (DLS). Due to the presence of the hydrophilic PMeOx block, the LCST was thus higher than that of the PiPrOx homopolymer (around body temperature).[35] Below the LCST, the copolymer proved fully soluble in water.

By increasing the temperature above the LCST, *i.e.* at 65 °C, the formation of well-defined micelles was first evidenced by DLS and transmission electron microscopy (TEM, Figure 1).

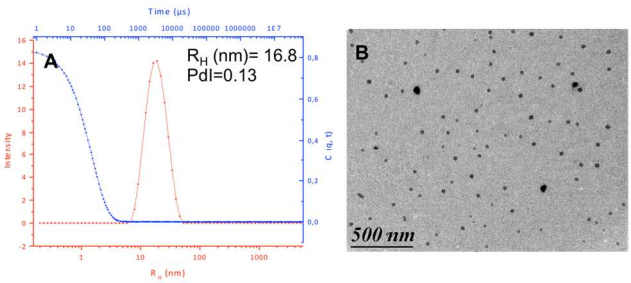

Figure 1 P(iPrOx$_{50}$-*b*-MeOx$_{50}$) micelle characterization at 65 °C: A) DLS analysis with correlogram and size distribution obtained at 90°; B) TEM micrograph (grid prepared at 65 °C)

Sizes thus obtained by DLS (R_H = 17 nm) and TEM image statistical analysis (r = 14 ± 2 nm) were in good agreement. Micelle formation above the LCST of the BCP was found reversible, only from an aqueous solution kept above the LCST for a short period of time (< 90 min). In these conditions, indeed, unimers were observed when the solution was cooled down to 25 °C, after heating at 65 °C, as followed by DLS.

Morphology evolution by crystallisation of P(iPrOx$_{50}$-*b*-MeOx$_{50}$)

In contrast, when the BCP aqueous solution was kept above the LCST for longer times, crystallisation occurred, but herein the presence of the hydrophilic stabilizing PMeOx block influenced the crystallisation process and the as-formed crystalline structures. The morphology evolution was monitored with time by *in situ* DLS measurements on a 10 mg/mL copolymer sample of P(iPrOx$_{50}$-*b*-MeOx$_{50}$) in water, at 65 °C. The initially well-defined and nearly monodisperse micelles progressively became unstable (Figure 2). Increase in polydispersity, scattering intensity and size was indeed observed, indicating that micelles evolved into larger and increasingly less defined structures.

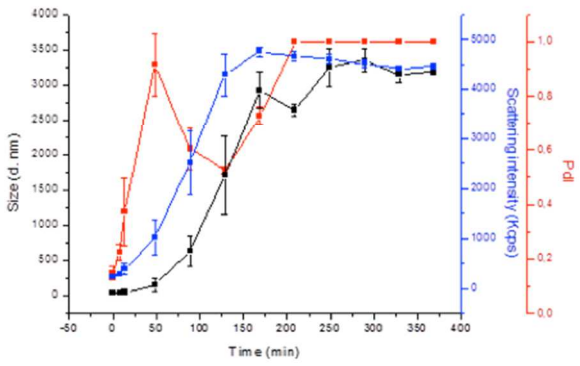

Figure 2 *In situ* DLS measurements of P(iPrOx$_{50}$-*b*-MeOx$_{50}$) in water (10 mg/mL; 65 °C)

The change in morphology also resulted in a change of the solution turbidity. Crystal formation could also be macroscopically detected. In order to obtain a better understanding of the assembly behaviour, aliquots were taken at different annealing times (90 min, 3h, 7h and 24h) and were allowed to cool down to room temperature. No significant change in the scattered intensity was observed by DLS, compared to the sample analysed *in situ* at 65 °C, suggesting that the previously formed nano/micro-objects were thermodynamically stable. Structures obtained at the different annealing times were further characterized by TEM (Figure 3). Withdrawn samples were deposited onto copper grid after cooling to room temperature, the nanostructures being supposedly 'locked', as suggested by DLS. Formation of a crystalline structure from the P(iPrOx-b-MeOx) BCP was clearly evidenced, with morphologies evolving with the annealing time. Intriguingly, some anisotropic fiber-like structures were observed after 90 min (Figure 3a), the proportion of which increased and appeared to arrange into denser "fiber-nodes", after 3h (Figure 3b). Nevertheless, some micellar nanostructures could also be observed (Figure 3c), suggesting that these micelles could experience a physically "core-crosslinking" phenomenon due to crystallisation. At longer annealing times (7h and 24h), the proportion of fibers further increased until network-like structures were achieved (Figure 3d and f). Yet, non-spherical crosslinked micelle-like nanostructures, around 30 nm in diameter, could still be detected (Figure 3e and g). We assumed that the aforementioned structures could coexist at each annealing time, but differed only in their proportion. Due to the length scale difference, however, all of

these structures could not be imaged at once. Our hypothesis is supported by the fact that crosslinked micelles were still detected even after 24 h, as part of the fiber-like structures (Figure 3g). It was thus highly likely that these primary crystalline nanostructures took part in the fiber formation.

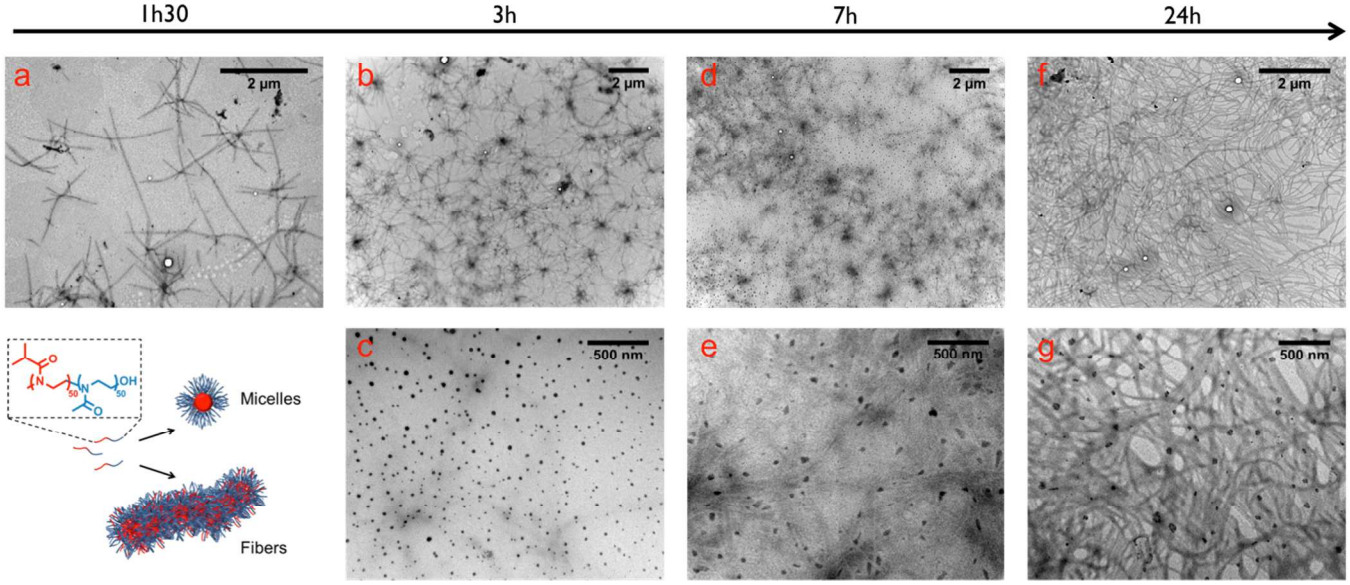

Figure 3 TEM micrographs of a 10 mg/mL of P(iPrOx$_{50}$-*b*-MeOx$_{50}$) solution in water heated at 65 °C for a) 1h30, b) and c) 3h, d) and e) 7h and f) and g) 24h

As the copolymer concentration was kept constant, progressive increase in the amount of crystalline materials, as determined by TEM, suggested that the extent of reversible micelles decreased proportionally. Thus, the self-assembled micelles might act as crystallisation seeds and the spatial restriction caused by the crystallisation of the PiPrOx block could result in the formation of spherical or distorted crosslinked micelles and fibers. A similar mechanism was described by O'Reilly *et al.* regarding the crystallisation-driven self-assembly of PLA-*b*-PPA BCP, where spherical micelles underwent crystallisation and nucleated the growth of cylindrical structures.[22]

The arrangement of the fibers seemed to evolve following specific steps. Firstly, individual growth was observed after which some fibers-nodes were found. As the proportion of fibers increased, inter-connection between fibers occurred leading, ultimately, to a more uniform fiber-like network (Figure 3f). TEM observations were in agreement with results delivered by DLS (Figure 2). Initially (in the first hour), an increase in polydispersity was noted, as individual anisotropic fibers were formed, which coexisted with a high number of reversible micelles (not observable by TEM prepared at room temperature). Subsequently, a reduction in the polydispersity was noted, corresponding to the formation of larger and more isotropic fiber-nodes shielding the smaller nanostructures. In a final step, an increase in polydispersity was again noted (upon formation of the fiber-like network).

Morphologies observed herein from the P(iPrOx$_{50}$-*b*-MeOx$_{50}$) BCP thus differed from those observed with the PiPrOx homopolymer, for which fibers initially formed and further assembled into micron-size spherical structures.[39] This difference can obviously be explained by the presence of the PMeOx block, forming a hydrophilic stabilizing shell. Cross-linked micelles were directly issued from the self-assembly of the BCP above its LCST, and the formation of a network -rather than a micro-spherical aggregated structure as observed by Schlaad *et al.*[37,39]- can be ascribed to the likely core-shell structure of the BCP fibers.

In order to monitor the crystal structure with time, the same aliquots were dried and analysed by wide angle X-ray scattering (WAXS; Figure 4).

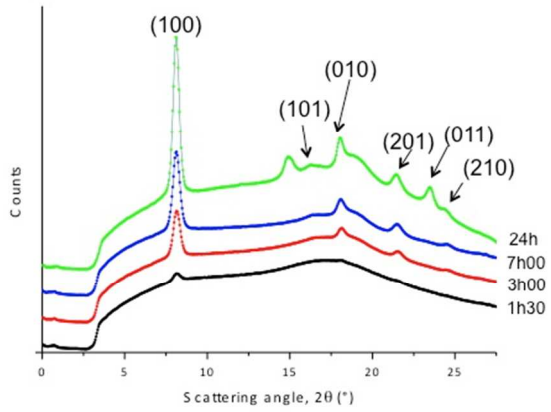

Figure 4 WAXS patterns of P(iPrOx$_{50}$-*b*-MeOx$_{50}$) after 1h40, 3h, 7h and 24h of annealing at 65 °C.

As in the case of the crystallisation of the PiPrOx homopolymer,[39] an amorphous halo was observed, and both the intensity and the sharpness of the crystalline peaks progressively increased, confirming that the BCP exhibited a semi-crystalline character. The majority of X-ray peaks could be easily assigned and were found to match those reported.[38,48] The two main peaks were observed at the same scattering angle as that of the homopolymer (2θ = 8° and 18.25° corresponding to d = 11.25 and 4.85 Å, respectively). Thus

the first crystalline structure was identical to that of PiPrOx homopolymer.[38]

Hydrophobic interactions above the LCST are expected to play a crucial role in the crystallisation phenomenon of our POx-based BCP. However, and as reported earlier, dipolar interactions could also be involved in the crystallisation process.[32,36,38] Solubility tests were carried out to investigate that point. BCP were first annealed for 24h at 65 °C, dried and dispersed in pure water or in a mixture of water and trifluoroacetic acid (TFA). In the former case, a turbid suspension was obtained, confirming that nanostructures remained intact, while in the water/TFA mixture, a clear solution was observed, suggesting that Van der Waals interactions were disrupted by TFA. In absence of TFA, the crystallisation mechanism may be similar to that proposed by Winnik *et al.*,[36] where hydrophobic interactions initially enable to arrange PiPrOx blocks close to each other, while the polymer chain shifts from trans and gauche conformations to an all trans conformation. This leads to the alignment of dipolar amide groups and the development of inter-chain dipolar interactions, thus favoring main chain crystallinity.[38]

Conclusions

The well-known crystallisation-driven self-assembly (CDSA) phenomenon has been applied for the first time to an all-oxazoline-based block copolymer (BCP) consisting of a hydrophilic poly(2-methyl-2-oxazoline) block and a crystallisable and thermo-sensitive poly(2-isopropyl-2-oxazoline) block. Well-defined and reversible micelle-like nanostructures are observed upon heating a P(iPrOx$_{50}$-*b*-MeOx$_{50}$) BCP to 65 °C, *i.e.* above the LCST of PiPrOx, for less than 90 min. When annealed for a period of time > 90 min, the crystallisation of PiPrOx leads to the formation of both spherical and distorted morphologies, including crystallised micelles and fibers. These structures eventually coexist at varying ratios as a function of the annealing time, and the longer the annealing time is, the higher the extent of crystallinity is. The initially formed micelle-like structures are eventually involved in fiber formation. Thus, by taking advantage of the BCP structure and the properties of each block, different morphologies can be achieved by CDSA, in comparison to those previously observed for the PiPrOx homopolymer, which is attributed to the stabilizing effect of the hydrophilic PMeOx block. Other P(iPrOx-*b*-MeOx) BCP with different compositions are currently evaluated, as a means to understand the key factors that affect structure formation. Likewise, change in the self-assembly protocol should also strongly influence morphologies observed.

Acknowledgements

The authors are grateful to the IDS FunMat program and the European commission for financial support. N. Guidolin, A.-L.Wirotius and A. Bentaleb are thanked for their assistance with SEC, NMR and WAXS analyses respectively.

Notes and references

[a] Université de Bordeaux/IPB, ENSCBP, 16 avenue Pey Berland, 33607 Pessac Cedex, France. taton@enscbp.fr, lecommandoux@enscbp.fr.

[b] CNRS, Laboratoire de Chimie des Polymères Organiques (UMR5629), Pessac, France.

[c] University of Waterloo, 200 University Avenue West, Waterloo, Ontario, Canada, N2L 3G1.

[d] University of Liège, Mammalian Cell Culture Laboratory, Allée de la Chimie 3 Sart Tilman, 4000 Liège, Belgium.

Electronic Supplementary Information (ESI) available: [NMR spectra, SEC trace, cloud point measurement, reversible micelles DLS characterization and distribution of micelle size by TEM, WAXS scattering angles and corresponding spacing between the crystallographic planes obtained from Bragg's law, picture of of P(iPrOx$_{50}$-*b*-MeOx$_{50}$) in pure water and in water/trifluoroacetic acid mixture]. See DOI: 10.1039/b000000x/

1 F. S. Bates, M. A. Hillmyer, T. P. Lodge, C. M. Bates, K. T. Delaney and G. H. Fredrickson, *Science (80-.).*, 2012, **336**, 434–40.
2 Y. Mai and A. Eisenberg, *Chem. Soc. Rev.*, 2012, **41**, 5969–85.
3 J. Schmelz, F. H. Schacher and H. Schmalz, *Soft Matter*, 2013, **9**, 2101.
4 W.-N. He and J.-T. Xu, *Prog. Polym. Sci.*, 2012, **37**, 1350–1400.
5 J. Schmelz, M. Karg, T. Hellweg and H. Schmalz, *ACS Nano*, 2011, **5**, 9523–9534.
6 J. Schmelz, D. Pirner, M. Krekhova, T. M. Ruhland and H. Schmalz, *Soft Matter*, 2013, **9**, 11173.
7 J. Schmelz, A. E. Schedl, C. Steinlein, I. Manners and H. Schmalz, *J. Am. Chem. Soc.*, 2012, **134**, 13217–14225.
8 L. Yin, T. P. Lodge and M. A. Hillmyer, *Macromolecules*, 2012, **45**, 9460–9467.
9 L. Yin and M. A. Hillmyer, *Macromolecules*, 2011, **44**, 3021–3028.
10 G. Molev, Y. Lu, K. S. Kim, I. C. Majdalani, G. Guerin, S. Petrov, G. Walker, I. Manners and M. A. Winnik, *Macromolecules*, 2014, **47**, 2604–2615.
11 M. Hsiao, S. Yusoff, M. A. Winnik and I. Manners, *Macromolecules*, 2014, **47**, 2361–2372.
12 L. Jia, L. Tong, Y. Liang, A. Petretic, G. Guerin, I. Manners and M. A. Winnik, *J. Am. Chem. Soc.*, 2014, DOI: 10.1021/ja510019s.
13 A. Nunns, G. R. Whittell, M. A. Winnik and I. Manners, *Macromolecules*, 2014, DOI: 10.1021/ma501725h.
14 N. McGrath, F. H. Schacher, H. Qiu, S. Mann, M. A. Winnik and I. Manners, *Polym. Chem.*, 2014, **5**, 1923.
15 J. B. Gilroy, D. J. Lunn, S. K. Patra, G. R. Whittell, M. A. Winnik and I. Manners, *Macromolecules*, 2012, **45**, 5806–5815.
16 A. M. Mihut, M. Drechsler, M. Möller and M. Ballauff, *Macromol. Rapid Commun.*, 2010, **31**, 449–53.
17 A. M. Mihut, J. J. Crassous, H. Schmalz, M. Drechsler and M. Ballauff, *Soft Matter*, 2012, **8**, 3163–3173.
18 A. M. Mihut, A. Chiche, M. Drechsler, H. Schmalz, E. Di Cola, G. Krausch and M. Ballauff, *Soft Matter*, 2009, **5**, 208–213.
19 A. M. Mihut, J. J. Crassous, H. Schmalz and M. Ballauff, *Colloid Polym. Sci.*, 2010, **288**, 573–578.
20 N. Petzetakis, A. P. Dove and R. K. O'Reilly, *Chem. Sci.*, 2011, **2**, 955.
21 N. Petzetakis, M. P. Robin, J. P. Patterson, E. G. Kelley, P. Cotanda, P. H. H. Bomans, N. a J. M. Sommerdijk, A. P. Dove, T. H. Epps and R. K. O'Reilly, *ACS Nano*, 2013, **7**, 1120–8.
22 N. Petzetakis, D. Walker, A. P. Dove and R. K. O'Reilly, *Soft Matter*, 2012, **8**, 7408.
23 L. Sun, N. Petzetakis, A. Pitto-barry, T. L. Schiller, N. Kirby, D. J. Keddie, B. J. Boyd, R. K. O. Reilly and A. P. Dove, *Macromolecules*, 2013, **46**, 9074–9082.

24 W. He, B. Zhou, J. Xu, B. Du and Z. Fan, *Macromolecules*, 2012, **45**, 9768–9778.
25 K. Rajagopal, A. Mahmud, D. a Christian, J. D. Pajerowski, A. E. X. Brown, S. M. Loverde and D. E. Discher, *Macromolecules*, 2010, **43**, 9736–9746.
26 W.-N. He, J.-T. Xu, B.-Y. Du, Z.-Q. Fan and X. Wang, *Macromol. Chem. Phys.*, 2010, **211**, 1909–1916.
27 R. M. Van Horn, J. X. Zheng, H.-J. Sun, M.-S. Hsiao, W.-B. Zhang, X.-H. Dong, J. Xu, E. L. Thomas, B. Lotz and S. Z. D. Cheng, *Macromolecules*, 2010, **43**, 6113–6119.
28 K. Aoi, H. Suzuki and M. Okada, *Macromolecules*, 1992, **25**, 7073–7075.
29 M. Barz, R. Luxenhofer, R. Zentel and M. J. Vicent, *Polym. Chem.*, 2011, **2**, 1900–1918.
30 K. Knop, R. Hoogenboom, D. Fischer and U. S. Schubert, *Angew. Chemie, Int. Ed.*, 2010, **49**, 6288–308.
31 M. Bauer, C. Lautenschlaeger, K. Kempe, L. Tauhardt, U. S. Schubert and D. Fischer, *Macromol. Biosci.*, 2012, **12**, 986–998.
32 H. Schlaad, C. Diehl, A. Gress, M. Meyer, A. Levent Demirel, Y. Nur and A. Bertin, *Macromol. Rapid Commun.*, 2010, **31**, 511–25.
33 R. Hoogenboom, *Macromol. Chem. Phys.*, 2007, **208**, 18–25.
34 R. Hoogenboom, *Angew. Chemie, Int. Ed.*, 2009, **48**, 7978–94.
35 H. Uyama and S. Kobayashi, *Chem. Lett.*, 1992, **9**, 1643–1646.
36 Y. Katsumoto, A. Tsuchiizu, X. Qiu and F. M. Winnik, *Macromolecules*, 2012, **45**, 3531–3541.
37 M. Meyer, M. Antonietti and H. Schlaad, *Soft Matter*, 2007, **3**, 430–431.
38 A. L. Demirel, M. Meyer and H. Schlaad, *Angew. Chem. Int. Ed. Engl.*, 2007, **46**, 8622–4.
39 C. Diehl, P. Černoch, I. Zenke, H. Runge, R. Pitschke, J. Hartmann, B. Tiersch and H. Schlaad, *Soft Matter*, 2010, **6**, 3784–3788.
40 C. Diehl and H. Schlaad, *Chem. Eur. J.*, 2009, **15**, 11469–11472.
41 N. Morimoto, R. Obeid, S. Yamane, F. M. Winnik and K. Akiyoshi, *Soft Matter*, 2009, **5**, 1597–1600.
42 M. M. Bloksma, M. M. R. M. Hendrix, U. S. Schubert and R. Hoogenboom, *Macromolecules*, 2010, **43**, 4654–4659.
43 P. T. Güner, A. Mikó, F. F. Schweinberger and A. L. Demirel, *Polym. Chem.*, 2012, **3**, 322–324.
44 E. F.-J. Rettler, H. M. L. Lambermont-Thijs, J. M. Kranenburg, R. Hoogenboom, M. V. Unger, H. W. Siesler and U. S. Schubert, *J. Mater. Chem.*, 2011, **21**, 17331–17337.
45 C. Diehl, I. Dambowsky, R. Hoogenboom and H. Schlaad, *Macromol. Rapid. Commun.*, 2011, **32**, 1753–1758.
46 M. Meyer and H. Schlaad, *Macromolecules*, 2006, **39**, 3967–3970.
47 K. Aoi and M. Okada, *Prog. Polym. Sci.*, 1996, **21**, 151–208.
48 M. Litt, F. Rhal and L. G. Roldan, *J. Polym. Sci. Part A-2 Polym. Phys.*, 1969, **7**, 463–473.

